PHYSICAL REVIEW A VOLUME 46, NUMBER 3 1 AUGUST 1992

Relativistic multichannel calculation of the Ne KLL and Ar $L_2M_{2,3}M_{2,3}$ Auger transition rates

J. Tulkki and T. Åberg
Laboratory of Physics, Helsinki University of Technology SF-02150 Espoo, Finland

A. Mäntykenttä and H. Aksela
Department of Physics, University of Oulu SF-90570 Oulu, Finland

(Received 21 January 1992)

The multichannel multiconfiguration Dirac-Fock method has been used to study the Ne KLL and Ar $L_2M_{2,3}M_{2,3}$ Auger-electron transitions. Final-state correlation effects are accounted for by simultaneously including several ionic configurations and ionization channels in the calculation of the final-state many-electron wave functions. Our computational approach is based on scattering theory, which properly accounts for the incoming wave boundary condition. The line intensities from our test calculation for Ne KLL transitions are in good agreement with earlier theoretical results and with experiment. The interchannel coupling is stronger for the final states of the Ar $L_2M_{2,3}M_{2,3}$ transitions, but the net effect on the line intensities is somewhat smaller than that for Ne. Even the most extensive multichannel calculations are not fully able to reproduce the measured total rate and the ratio of $^3P_{0,1,2}$ to $^1D_2$ transition rates. The remaining discrepancy in the branching ratios of Auger lines is attributed to the omission of initial-state configuration interaction, whereas the discrepancy between the measured and calculated total rates is suggested to be mainly due to the neglect of relaxation. Our results indicate that, in analogy to outer-shell photoionization, the final-state interchannel interaction does not in general affect the strongest Auger lines very much when the kinetic energy of the Auger electrons exceeds about 200 eV.

PACS number(s): 32.80.Hd, 32.80.Fb

I. INTRODUCTION

The nonradiative decay of an inner-shell hole usually results in several ionization channels corresponding to different angular momenta and spin of the Auger electron and to different final states of the doubly charged ion [1]. The interaction between different ionic configurations [final-ionic-state configuration interaction (FISCI)] and associated continuum states [final-continuum-state configuration interaction (FCSCI)] may lead to significant redistribution of intensity in the spectrum of the emitted electrons [2]. The electron spectrum is also influenced by other many-body effects such as initial-ionic-state configuration interaction (IISCI) and relaxation. The post-collision interaction (PCI) may have conspicious effects on Auger spectra in the near-threshold excitation region [3, 4] but they are not explored in this work. In the following we shall describe in detail the multichannel multiconfiguration Dirac-Fock (MMCDF) method which we have recently developed for calculation of near-threshold photoionization cross sections [5] and apply it to the study of final-state correlation effects in Ne KLL and Ar $L_2M_{2,3}M_{2,3}$ Auger spectra. The MMCDF method accounts for FISCI and FCSCI in a *unified* and *nonperturbative* way by combining configuration-interaction (CI) and channel-interaction (K-matrix) methods. Our approach has been especially tailored to serve as a general tool for the construction of many-electron wave functions of a system which consists of a many-electron ion and *one* continuum electron, independently of a particular excitation or decay mechanism. IISCI and relaxation can be included in our computational method on an *ab initio* basis but are excluded from the present calculations. In general the MMCDF method should be most effective in cases where strong correlation effects are confined to a rather small subsection of the total configuration and channel space. The relativistic effects are small in the Auger spectra discussed in this work. Using MMCDF the LS-coupled states are automatically obtained in the calculation as superpositions of jj-coupled configurations and channels.

Although the first nonrelativistic multichannel calculations of Auger transition rates were carried out more than a decade ago [6–8] there exist so far very few calculations based on this method or its relativistic extension. The cases studied were the Ne KLL Auger transitions [6, 7], as well as the Mg KLL, KLM, and KMM transitions [8]. The same scattering-theoretical method [1] was applied to a study of the intense $L_1L_{2,3}M_1$ Coster-Kronig transitions in Ar [9] and of the Ne KLL transitions using another numerical technique [10]. Recent studies of KLL spectra of neonlike ions [11], of the Kr L_3MM spectrum [12], and of the L-shell Auger spectra of Mg-like Al and Ar [13] involve a relativistic generalization of this method. The Ne KLL transitions have also been studied using an S-matrix [14] and a relativistic close-coupling approach [15]. Kelly calculated the partial and total Ne KLL rates using nonrelativistic many-body perturbation theory (MBPT) [16]. All these calculations agree in that interchannel coupling can change the spectral distribution of the Auger or Coster-Kronig electrons and reduce the sometimes very large discrepancies [9] between calculated and measured transition rates. For Ne and Mg the changes caused by the interchannel interaction are rather small for the strongest Auger lines (typically less than 10%) whereas the effect is much larger for the weak lines on a relative scale. In the Ar $L_1L_{2,3}M_1$ spectrum the interchannel effect is somewhat larger as expected on the basis of the low kinetic energy of the Coster-Kronig electrons [9]. The interchannel effects in the K-shell Auger spectra of Ne and Mg are somewhat surprising considering the high kinetic energy (700–1200 eV) of the emitted electrons. In calculations of photoionization cross sections we have found that the channel interactions become very small at kinetic energies of about 200 eV above the threshold [5].

These fairly succesful applications of the multichannel method and MBPT in the calculation of Auger spectra showed that inclusion of channel mixing can reduce the discrepancy between theory and experiment significantly. As a consequence, discrepancies between single-channel calculations and experiment have since then been often addressed to the exclusion of channel mixing. In this work we present a computational approach which can be used for a systematic study of these interactions. We will first describe the scattering-theoretical derivation of Auger rates with theoretical and numerical details in the Appendix. We have used the frequently studied Ne KLL Auger transitions as a test case to check the numerical accuracy of our code. We have also applied our method to Ar $L_2M_{2,3}M_{2,3}$ transitions where among existing discrepancies the intensity of the ${}^3P_{0,1,2}$ line as compared to the intensity of the ${}^1D_2$ line is clearly overestimated by the single-channel theory [17]. The electron energies of this Auger spectrum lie between 200 and 210 eV, which is only a fraction of the KLL transition energies in Ne and Mg. The interchannel interaction is therefore expected to be important in this spectrum.

II. THEORY

The derivation of nonrelativistic multichannel Auger rates from the first principles of scattering theory has been presented by Åberg and Howat [1]. The relativistic extension of their formalism is obtained by replacing the Hartree-Fock bound and continuum orbitals in the transition amplitudes by the corresponding Dirac-Fock orbitals. The theoretical basis of the MMCDF method, the computational approach and the structure of our computer code are described in the Appendix. The Breit interaction has been excluded from the matrix elements of interchannel interaction and from the transition amplitudes but can be included if important. In the following we have also neglected the coupling between radiative and nonradiative decay modes [1]. The multichannel Auger transition amplitude consequently is

$$\langle\Phi_0|H-E|\Phi^-_{\Gamma E}\rangle=\sum_{\alpha=1}^{N_c}\left(\langle\Phi_0|H-E|\phi_{\alpha E}\rangle+\sum_{\beta=1}^{N_c}\mathrm{P}\int dE'\frac{\langle\Phi_0|H-E|\phi_{\beta E'}\rangle\langle\phi_{\beta E'}|K|\phi_{\alpha E}\rangle}{E-E'}\right)Z^-_{\alpha\Gamma}, \tag{1}$$

where $|\Phi_0\rangle$ denotes the initial-state wave function and $|\Phi^-_{\Gamma E}\rangle$ the multichannel multiconfiguration final-state wave function. The single-channel transition amplitude is given by $\langle\Phi_0|H-E|\phi_{\alpha E}\rangle$ where H is the full electronic Hamiltonian, and as explained in the Appendix the coefficients $Z^-_{\alpha\Gamma}$ take full account of the incoming-wave boundary condition. The functions $\phi_{\alpha E}$ and $\phi_{\beta E'}$ are the multiconfiguration single-channel wave functions (A3). In the Appendix we show that the general scattering-theoretical result of Åberg and Howat [1] is equivalent to that of Starace [18] and that both lead to Eq. (1). In previous numerical calculations [6–13] different lower-order approximations of Eq. (1) have been used. Typically the K matrix (A9) has been set equal to the V matrix (A6) and $Z^-_{\alpha\Gamma}$ has been replaced by the unit matrix $\delta_{\alpha\Gamma}$. As will be seen below these approximations are only justified at high kinetic energies of the continuum electron. In the calculation of low-energy Auger or Coster-Kronig spectra the full multichannel wave function given by Eq. (A12) must not only be used in the calculation of angular distributions but also in the calculation of line intensities. In the calculation of angular distributions a superposition of the wave functions $|\Psi^-_{\Gamma E}\rangle$ must be introduced in order to fulfill the appropriate angle-resolved incoming-wave boundary conditions [1, 18]. In this work we will use a common orthogonal set of initial- and final-state orbitals which excludes relaxation effects. The single-channel transition amplitudes in Eq. (1) now become $\langle\Phi_0|H-E|\phi_{\alpha E}\rangle=\langle\Phi_0|\sum_{i<j}1/r_{ij}|\phi_{\alpha E}\rangle$. The relaxation effects [1] have been studied within the single-channel approximation in the case of Ne KLL [7] and Mg K [8] Auger transitions and have been found to be rather small except for some weak lines. In contrast, relaxation makes a large contribution to the Ar $L_1L_{2,3}M_1$ Coster-Kronig spectrum [19].

III. CALCULATIONS

A. Ne KLL transitions

The initial- and final-state wave functions were calculated by the multiconfiguration Dirac-Fock (MCDF) method using average level (AL) optimization [20]. For

TABLE I. Multiconfiguration atomic-state functions Ψ_α of the final doubly charged ion in Ne KLL transitions, and continuum orbitals $\chi_{\kappa\epsilon}$ which are needed for the construction of the corresponding multiconfiguration single-channel $J = 1/2$ wave functions. The symbols $\bar{l}$ and l distinguish between Dirac-Fock orbitals having $j = l - \frac{1}{2}$ and $j = l + \frac{1}{2}$, respectively.

Assignment	Wave function	Continuum orbital $\chi_{\kappa\epsilon}$
Ψ_1	$0.5637\vert 2s^2 2\bar{p}^1 2p^3, J = 2\rangle + 0.8260\vert 2s^2 2\bar{p}^2 2p^2, J = 2\rangle$	$\bar{d}, d$
Ψ_2	$\vert 2s^2 2\bar{p}^1 2p^3, J = 1\rangle$	$s, \bar{d}$
Ψ_3	$0.0029\vert 2s^0 2\bar{p}^2 2p^4, J = 0\rangle - 0.8062\vert 2s^2 2\bar{p}^0 2p^4, J = 0\rangle + 0.5917\vert 2s^2 2\bar{p}^2 2p^2, J = 0\rangle$	s
Ψ_4	$-0.8260\vert 2s^2 2\bar{p}^1 2p^3, J = 2\rangle + 0.5637\vert 2s^2 2\bar{p}^2 2p^2, J = 2\rangle$	$\bar{d}, d$
Ψ_5	$-0.1845\vert 2s^0 2\bar{p}^2 2p^4, J = 0\rangle - 0.5820\vert 2s^2 2\bar{p}^0 2p^4, J = 0\rangle - 0.7920\vert 2s^2 2\bar{p}^2 2p^2, J = 0\rangle$	s
Ψ_6	$\vert 2s^1 2\bar{p}^2 2p^3, J = 2\rangle$	$p, \bar{f}$
Ψ_7	$0.8138\vert 2s^1 2\bar{p}^1 2p^4, J = 1\rangle - 0.5811\vert 2s^1 2\bar{p}^2 2p^3, J = 1\rangle$	$\bar{p}, p$
Ψ_8	$\vert 2s^1 2\bar{p}^1 2p^4, J = 0\rangle$	$\bar{p}$
Ψ_9	$0.5811\vert 2s^1 2\bar{p}^1 2p^4, J = 1\rangle + 0.8138\vert 2s^1 2\bar{p}^2 2p^3, J = 1\rangle$	$\bar{p}, p$
Ψ_{10}	$0.9828\vert 2s^0 2\bar{p}^2 2p^4, J = 0\rangle - 0.1069\vert 2s^2 2\bar{p}^0 2p^4, J = 0\rangle - 0.1504\vert 2s^2 2\bar{p}^2 2p^2, J = 0\rangle$	s

the initial state we used the single-configuration $1s$-hole wave function. The final bound states of the Ne KLL transitions were calculated by including 10 jj-coupled configurations obtained from the $1s^2 2s^0 2p^6$, $1s^2 2s^1 2p^5$, and $1s^2 2s^2 2p^4$ double-hole parent configurations. In Table I we list the multiconfiguration atomic-state wave functions (ASF's) of the final doubly charged ion and all possible continuum orbitals that can be coupled to these ionic-state vectors to obtain the multiconfiguration single-channel wave functions, corresponding to the total angular momentum $J = 1/2$. This gives altogether 16 jj-coupled channels.

The transition rates were calculated using two different sets of bound and continuum orbitals. The first set (I) was constructed by optimizing the bound orbitals with respect to the initial state of the ion. These bound orbitals were also used for the final state to obtain the ionic-state vectors in a separate CI calculation. This gives state vectors that are slightly different from those listed in Table I which are based on orbitals (F) that are optimized with respect to the final state of the ion. The continuum orbitals were generated in the jj-average V^{N-2} potential constructed from either orbital set I or F. In both cases the electronic occupation numbers were set to correspond to the average electron distribution in the final doubly charged ion. Lagrangian multipliers were included to obtain orthogonality between bound and continuum orbitals. In Table II the single-channel calculation (1) and multichannel calculation (3) are based on orbital set I. The results obtained using the orbital set F for both initial and final states are labelled (2) and (4) in Table II. For the numerical evaluation of the multichannel rates (1) the channel-interaction matrix V [Eq. (A6)] must be tabulated as a function of the channel energy. In the Ne KLL case the Auger electrons are ejected with kinetic energies between 745 and 810 eV. A distribution of continuum orbital energies starting from 300 eV with a spacing of 30 eV for the first 33 points and a spacing of 200 eV for the last 8 points was found to provide solutions of the K-matrix equation (A8) and eigenchannel equation (A10) with a good numerical accuracy.

For comparison we also include some previous theoretical results in Table II. A comparison of our MMCDF results with the nonrelativistic multichannel calculation of Howat, Åberg, and Goscinski [7] and the relativistic close-coupling calculation (which effectively accounts for interchannel interactions) by Bruneau [15] we find that the influence of FCSCI is very similar. All multichannel calculations agree within 4%. Comparison between different relative partial rates shows that the $KL_1L_{2,3}$ ^3P

TABLE II. Neon KLL relative partial transition rates and absolute total transition rates in units of 10^{-3} a.u. The sum of the relative line intensities is normalized to 100.

Final state	Single-channel rate		Multichannel rate					Expt.[h]
	Calc.1[a]	Calc.2[b]	Calc.3[c]	Calc.4[d]	Calc.5[e]	Calc.6[f]	Calc.7[g]	
L_1L_1 ^1S (%)	8.35	8.16	6.37	6.03	6.1	5.7	6.0	6.2±0.3
$L_1L_{2,3}$ ^1P (%)	22.47	22.40	18.28	18.07	17.0	18.4	18.5	17.2±0.2
$L_1L_{2,3}$ ^3P (%)	9.71	7.09	9.46	6.82	6.1	9.6	8.4	6.3±0.2
$L_{2,3}L_{2,3}$ ^1S (%)	6.93	6.84	8.76	8.79	9.6	9.0	8.9	9.5±0.4
$L_{2,3}L_{2,3}$ ^1D (%)	52.53	55.50	57.12	60.27	61.2	57.3	58.1	60.9±0.2
$L_{2,3}L_{2,3}$ ^3P (%)	0.01	0.01	0.01	0.02				
Total rate (ma.u.)	10.29	7.93	10.31	7.95	8.05	10.57	9.77	9.9±0.7

[a] Single-channel calculation, basis set I.

[b] Single-channel calculation, basis set F.

[c] Multichannel calculation, basis set I.

[d] Multichannel calculation, basis set F.

[e] Nonrelativistic many-body perturbation theory (Ref. [16]).

[f] Nonrelativistic multichannel calculation (Ref. [7]).

[g] Relativistic close-coupling approach (Ref. [15]).

[h] Refs. [21–23].

and $KL_{2,3}L_{2,3}\ ^1D$ transition rates depend mostly on the choice of the orbital set. The change from one basis to another has an essential effect on the total KLL transition rate. Instead FCSCI changes the total rate very little even if the relative rates of individual lines change considerably. Table II shows that when FCSCI is taken into account the calculations are, independently of the choice of the basis set, in a better agreement with the experiment than the single-channel results.

The experimental absolute value of the total rate in Table II is based on a $1s$ linewidth of 0.27±0.02 eV [21]. The experimental relative line intensities are taken from a recent high-resolution work [22]. The error limits were obtained by comparing these intensities with our own high-resolution results [23]. The total experimental width in Table II is reproduced to experimental accuracy by calculations (1) and (3), based on orbital set I. The same is true for the rates (6) and (7) which were also obtained using bound orbitals which were optimized with respect to the initial state. Multichannel calculations based on orbital set F (calculation 4 in Table II) reproduce the relative line intensities fairly well but underestimate the

TABLE III. Multiconfiguration atomic-state functions Ψ_α of the final doubly charged ion in Ar $L_2M_{2,3}M_{2,3}$ transitions, and continuum orbitals $\chi_{\kappa\epsilon}$ which are needed for the construction of the corresponding multiconfiguration single-channel $J = 1/2$ wave functions. The symbols $\bar{l}$ and l distinguish between Dirac-Fock orbitals having $j = l - \frac{1}{2}$ and $j = l + \frac{1}{2}$, respectively.

Assignment	Wave function	Continuum orbital $\chi_{\kappa\epsilon}$
Ψ_1	$0.7849\vert 3s^2 3\bar{p}^0 3p^4, J = 0\rangle - 0.6088\vert 3s^2 3\bar{p}^2 3p^2, J = 0\rangle - 0.0079\vert 3s^0 3\bar{p}^2 3p^4, J = 0\rangle$ $+0.0410\vert[(3s^1 3\bar{p}^1, J = 0)3p^3, J = 3/2]3\bar{d}^1, J = 0\rangle$ $+0.0748\vert[(3s^1 3\bar{p}^1, J = 1)3p^3, J = 3/2]3\bar{d}^1, J = 0\rangle$ $+0.0769\vert[(3s^1 3\bar{p}^1, J = 1)3p^3, J = 5/2]3d^1, J = 0\rangle$ $-0.0080\vert[(3s^1 3\bar{p}^2, J = 1/2)3p^2, J = 3/2]3\bar{d}^1, J = 0\rangle$ $+0.0052\vert[(3s^1 3\bar{p}^2, J = 1/2)3p^2, J = 5/2]3d^1, J = 0\rangle$	$\bar{p}$
Ψ_2	$-0.5395\vert 3s^2 3\bar{p}^1 3p^3, J = 2\rangle - 0.8420\vert 3s^2 3\bar{p}^2 3p^2, J = 2\rangle$	$p, \bar{f}$
Ψ_3	$\vert 3s^2 3\bar{p}^1 3p^3, J = 1\rangle$	$\bar{p}, p$
Ψ_4	$0.8420\vert 3s^2 3\bar{p}^1 3p^3, J = 2\rangle - 0.5395\vert 3s^2 3\bar{p}^2 3p^2, J = 2\rangle$	$p, \bar{f}$
Ψ_5	$0.6029\vert 3s^2 3\bar{p}^0 3p^4, J = 0\rangle + 0.7760\vert 3s^2 3\bar{p}^2 3p^2, J = 0\rangle + 0.1850\vert 3s^0 3\bar{p}^2 3p^4, J = 0\rangle$ $+0.0109\vert[(3s^1 3\bar{p}^1, J = 0)3p^3, J = 3/2]3\bar{d}^1, J = 0\rangle$ $+0.0107\vert[(3s^1 3\bar{p}^1, J = 1)3p^3, J = 3/2]3\bar{d}^1, J = 0\rangle$ $-0.0109\vert[(3s^1 3\bar{p}^1, J = 1)3p^3, J = 5/2]3d^1, J = 0\rangle$ $-0.0084\vert[(3s^1 3\bar{p}^2, J = 1/2)3p^2, J = 3/2]3\bar{d}^1, J = 0\rangle$ $+0.0108\vert[(3s^1 3\bar{p}^2, J = 1/2)3p^2, J = 5/2]3d^1, J = 0\rangle$	$\bar{p}$
Ψ_6	$-\vert 3s^1 3\bar{p}^2 3p^3, J = 2\rangle$	$\bar{d}, d$
Ψ_7	$0.8089\vert 3s^1 3\bar{p}^1 3p^4, J = 1\rangle - 0.5880\vert 3s^1 3\bar{p}^2 3p^3, J = 1\rangle$	$s, \bar{d}$
Ψ_8	$\vert 3s^1 3\bar{p}^1 3p^4, J = 0\rangle$	s
Ψ_9	$0.5880\vert 3s^1 3\bar{p}^1 3p^4, J = 1\rangle + 0.8089\vert 3s^1 3\bar{p}^2 3p^3, J = 1\rangle$	$s, \bar{d}$
Ψ_{10}	$0.0870\vert 3s^2 3\bar{p}^0 3p^4, J = 0\rangle + 0.1270\vert 3s^2 3\bar{p}^2 3p^2, J = 0\rangle - 0.7366\vert 3s^0 3\bar{p}^2 3p^4, J = 0\rangle$ $-0.2691\vert[(3s^1 3\bar{p}^1, J = 0)3p^3, J = 3/2]3\bar{d}^1, J = 0\rangle$ $-0.1767\vert[(3s^1 3\bar{p}^1, J = 1)3p^3, J = 3/2]3\bar{d}^1, J = 0\rangle$ $+0.4031\vert[(3s^1 3\bar{p}^1, J = 1)3p^3, J = 5/2]3d^1, J = 0\rangle$ $+0.2131\vert[(3s^1 3\bar{p}^2, J = 1/2)3p^2, J = 3/2]3\bar{d}^1, J = 0\rangle$ $-0.3495\vert[(3s^1 3\bar{p}^2, J = 1/2)3p^2, J = 5/2]3d^1, J = 0\rangle$	$\bar{p}$
Ψ_{11}	$0.0030\vert 3s^2 3\bar{p}^0 3p^4, J = 0\rangle + 0.0065\vert 3s^2 3\bar{p}^2 3p^2, J = 0\rangle - 0.0338\vert 3s^0 3\bar{p}^2 3p^4, J = 0\rangle$ $+0.6721\vert[(3s^1 3\bar{p}^1, J = 0)3p^3, J = 3/2]3\bar{d}^1, J = 0\rangle$ $-0.5534\vert[(3s^1 3\bar{p}^1, J = 1)3p^3, J = 3/2]3\bar{d}^1, J = 0\rangle$ $+0.2133\vert[(3s^1 3\bar{p}^1, J = 1)3p^3, J = 5/2]3d^1, J = 0\rangle$ $+0.3357\vert[(3s^1 3\bar{p}^2, J = 1/2)3p^2, J = 3/2]3\bar{d}^1, J = 0\rangle$ $+0.2872\vert[(3s^1 3\bar{p}^2, J = 1/2)3p^2, J = 5/2]3d^1, J = 0\rangle$	$\bar{p}$
Ψ_{12}	$-0.0011\vert 3s^2 3\bar{p}^0 3p^4, J = 0\rangle + 0.0107\vert 3s^2 3\bar{p}^2 3p^2, J = 0\rangle - 0.0420\vert 3s^0 3\bar{p}^2 3p^4, J = 0\rangle$ $-0.4752\vert[(3s^1 3\bar{p}^1, J = 0)3p^3, J = 3/2]3\bar{d}^1, J = 0\rangle$ $+0.0272\vert[(3s^1 3\bar{p}^1, J = 1)3p^3, J = 3/2]3\bar{d}^1, J = 0\rangle$ $+0.2738\vert[(3s^1 3\bar{p}^1, J = 1)3p^3, J = 5/2]3d^1, J = 0\rangle$ $+0.1100\vert[(3s^1 3\bar{p}^2, J = 1/2)3p^2, J = 3/2]3\bar{d}^1, J = 0\rangle$ $+0.8274\vert[(3s^1 3\bar{p}^2, J = 1/2)3p^2, J = 5/2]3d^1, J = 0\rangle$	$\bar{p}$
Ψ_{13}	$-0.0740\vert 3s^2 3\bar{p}^0 3p^4, J = 0\rangle + 0.0511\vert 3s^2 3\bar{p}^2 3p^2, J = 0\rangle + 0.0035\vert 3s^0 3\bar{p}^2 3p^4, J = 0\rangle$ $+0.3036\vert[(3s^1 3\bar{p}^1, J = 0)3p^3, J = 3/2]3\bar{d}^1, J = 0\rangle$ $+0.2682\vert[(3s^1 3\bar{p}^1, J = 1)3p^3, J = 3/2]3\bar{d}^1, J = 0\rangle$ $+0.6717\vert[(3s^1 3\bar{p}^1, J = 1)3p^3, J = 5/2]3d^1, J = 0\rangle$ $-0.6131\vert[(3s^1 3\bar{p}^2, J = 1/2)3p^2, J = 3/2]3\bar{d}^1, J = 0\rangle$ $+0.0242\vert[(3s^1 3\bar{p}^2, J = 1/2)3p^2, J = 5/2]3d^1, J = 0\rangle$	$\bar{p}$
Ψ_{14}	$0.0595\vert 3s^2 3\bar{p}^0 3p^4, J = 0\rangle - 0.0403\vert 3s^2 3\bar{p}^2 3p^2, J = 0\rangle - 0.0065\vert 3s^0 3\bar{p}^2 3p^4, J = 0\rangle$ $-0.2467\vert[(3s^1 3\bar{p}^1, J = 0)3p^3, J = 3/2]3\bar{d}^1, J = 0\rangle$ $-0.7260\vert[(3s^1 3\bar{p}^1, J = 1)3p^3, J = 3/2]3\bar{d}^1, J = 0\rangle$ $-0.1542\vert[(3s^1 3\bar{p}^1, J = 1)3p^3, J = 5/2]3d^1, J = 0\rangle$ $-0.6186\vert[(3s^1 3\bar{p}^2, J = 1/2)3p^2, J = 3/2]3\bar{d}^1, J = 0\rangle$ $+0.0158\vert[(3s^1 3\bar{p}^2, J = 1/2)3p^2, J = 5/2]3d^1, J = 0\rangle$	$\bar{p}$
Ψ_{15}	$-0.0625\vert 3s^2 3\bar{p}^0 3p^4, J = 0\rangle - 0.0840\vert 3s^2 3\bar{p}^2 3p^2, J = 0\rangle + 0.6482\vert 3s^0 3\bar{p}^2 3p^4, J = 0\rangle$ $-0.3084\vert[(3s^1 3\bar{p}^1, J = 0)3p^3, J = 3/2]3\bar{d}^1, J = 0\rangle$ $-0.2387\vert[(3s^1 3\bar{p}^1, J = 1)3p^3, J = 3/2]3\bar{d}^1, J = 0\rangle$ $+0.4858\vert[(3s^1 3\bar{p}^1, J = 1)3p^3, J = 5/2]3d^1, J = 0\rangle$ $+0.2662\vert[(3s^1 3\bar{p}^2, J = 1/2)3p^2, J = 3/2]3\bar{d}^1, J = 0\rangle$ $-0.3314\vert[(3s^1 3\bar{p}^2, J = 1/2)3p^2, J = 5/2]3d^1, J = 0\rangle$	$\bar{p}$

total rate. A very good agreement is also obtained by the MBPT method (calculation 5 in Table II) which however gives a too low total rate in analogy to our calculations (2) and (4). We have also studied the effect of using the V matrix instead of the K matrix and of replacing the incoming-wave phase matrix Z^- [Eq. (A11)] by the unit matrix in the transition amplitudes. It was found that these approximations change the relative line intensities by less than 1%. In their calculations Howat, Åberg, and Goscinski [7] also neglected some of the intrachannel interactions. We found however that these residual terms have a very small effect on the line intensities. On the basis of these test calculations it can be concluded that our code is working with good numerical accuracy.

B. Ar $L_2M_{2,3}M_{2,3}$ transitions

The basic procedure in the case of Ar $L_2M_{2,3}M_{2,3}$ transitions was the same as for Ne. For Ar we carried out several calculations by gradually increasing the number of final-state configurations and channels. In the lowest-order approximation (1) we only included $3s^23p^4$, $J = 0,1,2$ parent final states. By coupling these with the Auger electron orbitals we obtain 8 jj-coupled channels. Second (2) we also included the $3s^03p^6$, $J = 0$ and $3s^13p^5$, $J = 0,1,2$ parent states which gives 16 channels. Finally (3) the $3s^13p^43d^1$, J=0 parent states were added which results in 21 channels. Our calculations indicated that the inclusion of the channels corresponding to the $3s^13p^43d^1$, $J = 1,2$ states did not significantly alter the results of the 21-channel calculation. The ionic-state vectors and the ionization channels of our 21-channel calculation are listed in Table III. The single-channel (calculations 1 to 3) and multichannel (calculations 5 to 7) transition rates are given in Table IV together with previous theoretical and experimental data. The above three calculations were performed using bound-state orbitals which were optimized with respect to the final state except for the 8-channel calculation. In this case bound orbitals which were optimized with respect to the initial state of the ion were also used (calculations 4 and 8 in Table IV).

In calculations (1) and (2) the bound orbitals were obtained from an AL MCDF calculation [20]. In calculation (3) we first carried out a MCDF calculation including the 15 possible states which can be obtained from the configurations and J values that are listed in Table III. The bound orbitals were taken from this calculation except for the $3d$ orbitals. The $3d$ orbitals were recalculated as follows: we first constructed a jj-average frozen core V^{N-2} potential excluding the $3d$ orbitals. The Dirac-Fock equation for the $3d$ electrons was then solved using this potential which was also used for the generation of the continuum orbitals. This procedure was necessary, since we found that when the $3d$ orbitals were taken from the ordinary MCDF calculation the Lagrangian multipliers between the $3d$ and the continuum orbitals became anomalously large. This led to a distortion of the continuum orbitals and to artificial transition rates. A separate calculation of the $3d$ orbitals as described above eliminates this artifact. The ionic-state vectors listed in Table III are based on the recalculated $3d$ orbitals. The Ar $L_2M_{2,3}M_{2,3}$ transitions energies are between 202 and 209 eV. The continuum orbitals which are needed for the solution of the MMCDF equations in the Appendix were calculated at 41 energies starting from 1 eV. A spacing of 12 eV was used between the first 33 points and a spacing of 90 eV between the last 8 points.

There is a close analogy of FISCI effects in the Ne KLL and Ar $L_2M_{2,3}M_{2,3}$ transitions as far as the s and p electrons are concerned. The most important configurations are obtained by distributing two holes in the Ne $2s, 2p$ and Ar $3s, 3p$ subshells, respectively. The coefficients of the state vectors obtained from the CI calculations including the resulting ten jj-coupled double-hole configurations agree within 10% for Ne and Ar. A remarkable difference exists, however, between FISCI in these final states which is due to the strong coupling of

TABLE IV. Argon $L_2M_{2,3}M_{2,3}$ relative transition rates. The sum of the relative line intensities is normalized to 100. The $L_2M_{2,3}M_{2,3}$ group rates and the L_2MM total rates are given in units of 10^{-3} a.u.

Final state	Single-channel rate				Multichannel rate					Expt.[f]
	Calc.1[a]	Calc.2[b]	Calc.3[c]	Calc.4[d]	Calc.5[a]	Calc.6[b]	Calc.7[c]	Calc.8[d]	Calc. 9[e]	
$^1S_0$ (%)	11.38	10.03	9.86	10.89	10.33	8.92	8.72	10.34	10.51	15.0±2.0
$^1D_2$ (%)	43.08	43.78	43.85	40.75	43.95	44.94	45.21	41.70	43.06	47.9±0.4
$^3P_{0,1,2}$(%)	45.54	46.19	46.29	48.36	45.72	46.14	46.34	47.96	46.43	37.1±0.4
Group rate (ma.u.)	3.94	3.88	3.87	4.98	4.11	4.39	4.40	5.15	4.81	3.0±0.7
Total rate (ma.u.)		5.24	5.24			5.78	5.80		6.43	4.4±0.7

[a] $3s^23p^4$ $J = 0,1,2$ (8 channels in calculation 5).

[b] $3s^23p^4$, $3s^03p^6$, $3s^13p^5$ $J = 0,1,2$ (16 channels in calculation 6).

[c] $3s^23p^4$, $3s^03p^6$, $3s^13p^5$ $J = 0,1,2$ and $3s^13p^43d^1$ $J = 0$ (21 channels in calculation 7).

[d] 8 channels, initial ionic state basis.

[e] Single-channel calculation, Ref. [17].

[f] Refs. [25–30].

the Ar $3s^0 3p^6$ configuration with the $3s^1 3p^4 3d$ configuration. This leads, especially when the coupling between the $3s^1 3p^5$ and $3s^2 3p^3 3d$ configurations is also included, to a very complicated line structure in the Ar $L_2 M_1 M_{2,3}$ and $L_2 M_1 M_1$ spectra [17, 24]. We have not been able to identify separate lines in this part of the spectrum and therefore we have limited ourselves to the analysis of the $L_2 M_{2,3} M_{2,3}$ spectrum. As can be seen from the single-channel results in Table IV these transitions are rather insensitive to the increase of the number of configurations. The strongest effect can be found for the $L_2 M_{2,3} M_{2,3}\ {}^1S_0$ line. This is predominantly due to the mixing between $3s^2 3p^4\ J = 0$ and $3s^0 3p^6\ J = 0$ states in analogy to a similar well-known mixing between $2s^2 2p^4$ and $2s^0 2p^6$ states in Ne. The inclusion of the $3s^1 3p^4 3d^1\ J = 0$ states does not change the single channel rates very much because these states do not have nonzero transition matrix elements with the initial ionic state. These states can only contribute to the single-channel rates by changing the mixing coefficients slightly in the final ionic states.

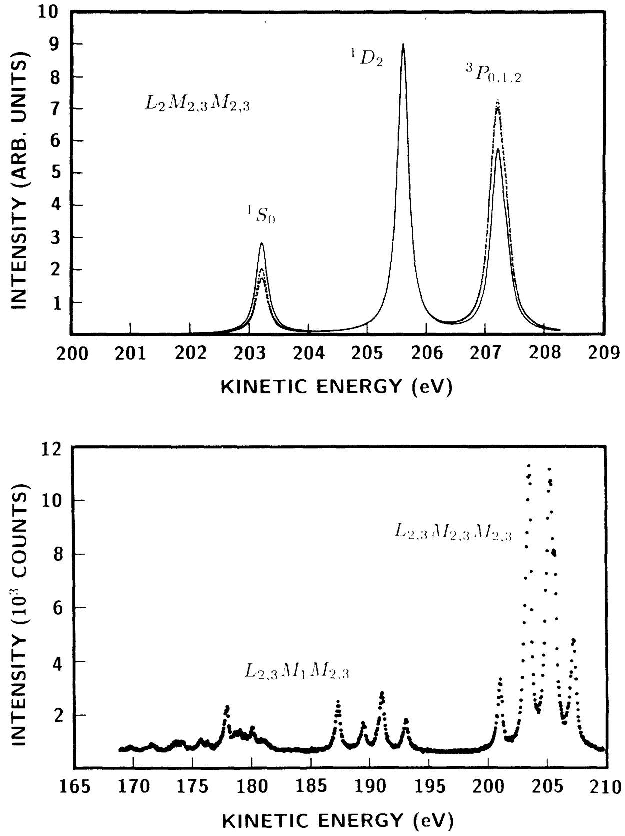

FIG. 1. Upper part: Experimental [23] and theoretical $L_2 M_{2,3} M_{2,3}$ Auger electron spectra of argon. The line positions have been determined experimentally. The experimental intensity distribution is indicated by the solid line. The dotted line represents the 15-configuration single-channel calculation (Calc. 3 in Table IV) and the dashed line the corresponding 21-channel calculation (Calc. 7 in Table IV). The theoretical spectra have been normalized at the maximum of the experimental $^1D_2$ line. Lower part: $L_{2,3}MM$ Auger spectrum of Ar [29]. The $L_2 M_{2,3} M_{2,3}$ spectrum was chosen for a detailed study since it consists of reliably identified lines making a comparison with theory feasible.

The comparison of the single and multichannel rates in Table IV shows that changes mainly take place in the transitions to the $^1D_2$ and $^1S_0$ final states. At the same time the relative rate of the $L_2 M_{2,3} M_{2,3}\ {}^3P_{0,1,2}$ transition is hardly affected by FCSCI. The effect of the choice of the orbital basis is similar to Ne; the total rate increases when we use orbitals optimized with respect to the initial state. In contrast to Ne, however, the total rate is also increased due to FCSCI.

The experimental total L_2 rate of Ar is obtained from the corresponding width of 0.12 ± 0.02 eV which agrees with the accepted L_3 width [2]. Data from high-resolution x-ray emission [25] and electron-energy loss [26] spectra support this value although some earlier low-resolution results [27, 28] point at a somewhat lower value of 0.10 eV. All data are however within the error limits. The $L_2 M_{2,3} M_{2,3}$ group rate was determined from the Auger line distribution obtained in a synchrotron-radiation experiment [29] in which the satellites originating from the 2s ionization were suppressed. The corresponding spectrum is shown in the lower part of Fig. 1.

The comparison between experimental and calculated values of the total rates shows that all calculations overestimate both the total rate and the group rate. The 21-channel calculation gives the best agreement.

The relative intensities given in the last column of Table IV are our own high-resolution results [23]. Error limits are obtained from the difference between our values and those reported in the literature [30]. Due to the strong overlap between the $L_2 M_{2,3} M_{2,3}(^1S_0)$ and $L_3 M_{2,3} M_{2,3}(^1D_2)$ lines the error limit is large for the weakest $^1S_0$ line. A comparison between experiment and theory shows that the theory overestimates the $^3P_{0,1,2}$ relative rate but underestimates the $^1D_2$ and $^1S_0$ rates, respectively. This is shown in the upper part of Fig. 1 where we compare experimental and calculated spectra. FCSCI does not remove the discrepancy as is visualized by the difference between the solid (experimental) and dashed (21-channel calculation) lines.

IV. CONCLUSIONS

The present study of final-state channel interaction leads to the unexpected result that this effect is stronger in the 800-eV Ne KLL than in the 200-eV Ar $L_2 M_{2,3} M_{2,3}$ Auger spectrum. This surprising observation is in contradiction with our studies of channel-interaction effects in valence-shell photoionization which show that interchannel matrix elements become negligible at kinetic energies of about 200 eV above threshold [5]. Our results also contradict the intuitive belief that the doubly charged final ionic field would in distinction to the singly charged ionic field in photoionization tend to reduce final-state correlation effects including the channel interaction. In order to understand this anomalous behavior we have studied how the K-matrix elements and single-channel amplitudes influence the partial amplitudes in Eq. (1).

For Ne we found that some weak lines (like $KL_{2,3}L_{2,3}\ {}^1S$) are strongly coupled through the interchannel interaction with lines that have a large intensity. This leads to relatively large changes in the intensity of the weak lines. In Ar $L_2M_{2,3}M_{2,3}$ spectrum we found that the weak ${}^1S_0$ line is not coupled with the strong ${}^1D_2$ and ${}^3P_{0,1,2}$ lines. Consequently the line intensities are not changed as much as in Ne. In both spectra we found that the total channel-interaction effect comes from several partial amplitudes without a single dominating one.

In contrast to Ne KLL the channel interaction causes a significant increase of the total Ar $L_2M_{2,3}M_{2,3}$ transition rate. This indicates that there is no "sum rule" that would preserve the total rate while the Auger intensity is redistributed as a result of the interchannel interaction. On the basis of present calculations it is too early to state any general rules based on known properties of one-electron orbitals or of many-body effects which could be used to obtain a lowest-order estimate of the effect of channel interaction on the Auger spectra. Since the overall strength of channel interaction is defined by two-electron Coulomb integrals involving the continuum orbitals of the ionized electrons it is likely to be larger in any low-kinetic-energy spectra or when the penetration of the centrifugal barrier becomes possible. The fact that single-channel calculations have been found to reproduce the spectral distribution surprisingly well in many high-energy closed-shell and nearly-closed-shell Auger spectra [31] supports the conclusion that in general the channel interaction does not affect the intensity distribution in Auger spectra very much if the kinetic energies exceed about 200 eV. This energy corresponds to the kinetic energy of Auger electrons in the Ar $L_2M_{2,3}M_{2,3}$ spectrum in which the relative intensity of the weakest ${}^1S_0$ line exhibits the largest change of about 10%. According to our view the Ne KLL spectrum is thus one of the exceptions of this general rule. In this case constructive interference between partial channel-interaction amplitudes leads to significant changes in the intensities of weak lines.

The present and many previous calculations have singled out FISCI as the dominating correlation effect in the intensity distribution of Auger spectra. The IISCI, although presumably less important for deep inner-shell one-hole states in closed-shell atoms, can also make a significant contribution as pointed out by Kelly [16]. The inclusion of IISCI in the MMCDF Auger amplitudes is possible on an *ab initio* basis and we expect to be able to present studies of this effect in the near future. The calculated total rates depend rather much on the choice of the orbital basis set. This indicates that relaxation may have a large effect on these spectra. Therefore a complete account of relaxation in the transition amplitudes is very important. Work in this direction is in progress and will be reported separately [32].

ACKNOWLEDGMENT

This work has been supported by the Academy of Finland.

APPENDIX: MULTICHANNEL MULTICONFIGURATION DIRAC-FOCK METHOD: THEORY AND NUMERICAL APPROACH

In this appendix we summarize the theoretical foundation of the MMCDF method and describe the numerical approach used in our computer code. The MMCDF approach is a combination of configuration-interaction and K-matrix methods. The following derivation of the MMCDF equations underlines their independence of a particular excitation or decay mechanism. The resulting wave functions can be used to account for final-state interactions in a variety of atomic collision processes. Although the continuum electron is called an Auger electron in the following our description applies, for example, to photoionization as well. The present version of our code can be applied to calculate correlated many-electron wave functions for any system which consists of an ion (atom) and *one* excited continuum electron. Our Hamiltonian and wave functions are explicitly relativistic, but the multichannel formalism is equally applicable to the nonrelativistic case.

The construction of the MMCDF wave functions is carried out in two steps. First we account for bound-state correlation effects by constructing a multiconfiguration wave function of the ion using the MCDF method [20]. Second the total wave function including both the ion and the Auger electron is calculated using the multichannel method. The single-configuration atomic-state function is denoted by $|\psi_{\alpha JM}\rangle$, where the index α identifies the configuration, the angular momenta, and their coupling. The multiconfiguration ASF of the ion is given by the linear superposition

$$|\Psi_\beta\rangle = \sum_{\alpha=1}^{N_f} C_\alpha^\beta |\psi_\alpha\rangle, \tag{A1}$$

where the sum is taken over N_f ionic configurations. In Eq. (A1) we have for brevity combined the quantum numbers βJM into one index β. The coefficients C_α^β and the one-electron orbitals of the Slater determinants in Eq. (A1) are usually optimized with respect to the final ionic states using the MCDF method. In the case of Auger transitions orbitals optimized with respect to the initial state are also used to simulate the effect of orbital relaxation. The CI wave function in Eq. (A1) is a solution of the wave equation

$$\langle\psi_\alpha|H^{\text{ion}} - E_\beta|\Psi_\beta\rangle = 0 \tag{A2}$$

for $\alpha = 1, \ldots, N_f$.

We define the multiconfiguration single-channel state as a properly coupled antisymmetrized product

$$|\phi_{\beta\kappa EJM}\rangle = \mathcal{A}\{|\Psi_\beta\rangle|\chi_{\kappa\varepsilon}\rangle\}, \tag{A3}$$

where $|\chi_{\kappa\varepsilon}\rangle$ is the continuum orbital corresponding to the quantum number $\kappa = (2j+1)(\ell - j)$ and the kinetic energy ε. The continuum orbitals are energy normalized and for the asymptotic phase we use the same convention as Rose [33]. The total energy associated with each single-channel state is a sum of the energy of the ion and the kinetic energy of the Auger electron: $E = E_\beta^{\rm ion} + \varepsilon$. For brevity we again use the notation βE instead of $\beta\kappa EJM$ in the following. The energy normalized continuum orbitals in Eq. (A3) are calculated in an average frozen-core field of the ASF's in Eq. (A1) by including Lagrangian multipliers to obtain an orthogonal set of discrete and continuum final-state orbitals. The average frozen core in the field of which the continuum orbitals are generated can be constructed in several different ways. The corresponding residual intrachannel correction terms are accounted for in the diagonalization of the multichannel wave equation as described below. In our calculations we have used the same frozen-core potential for all channels, because this procedure results in a fully orthogonal set of all final-state orbitals.

In analogy to Eq. (A1) the multichannel multiconfiguration wave function $|\Phi_{\Gamma E}\rangle$ is obtained as a linear combination of the single-channel wave functions (A3) integrated over energy. We have

$$|\Phi_{\Gamma E}\rangle = \sum_{\beta=1}^{N_c} \int b_{\beta\Gamma}(E', E)|\phi_{\beta E'}\rangle dE', \tag{A4}$$

where the integral includes a sum over Rydberg states associated with each ionization channel and N_c is the number of ionization channels. In analogy to the CI equation (A2) the wave equation now becomes

$$\langle\phi_{\alpha E'}|H - E|\Phi_{\Gamma E}\rangle = 0, \tag{A5}$$

where $\alpha = 1, \ldots, N_c$ and H is the combined Hamiltonian of the ion and the Auger electron.

In order to solve Eq. (A5) we first define the *residual interaction* V by

$$\langle\phi_{\alpha E''}|H - E|\phi_{\beta E'}\rangle = (E' - E)\delta(E'' - E')\delta_{\alpha\beta} + V_{\alpha\beta}(E''E'), \tag{A6}$$

which in general not only includes the nondiagonal interchannel interaction matrix elements but also some diagonal ($\alpha = \beta$) intrachannel elements. The latter matrix elements depend on Slater integrals which account for the difference between the frozen-core potential that is used to generate the set of continuum orbitals in the wave functions (A3) and the exact term-dependent frozen-core Dirac-Fock potential. This potential accounts for the interactions that are related to the coupling between the Auger electron and the ion and which in general are different for each ionization channel. In our code the intrachannel matrix elements are obtained by first calculating those Slater integrals which appear in the expression of the Koopmans energy for the continuum orbital [34]. Second these integrals are substracted from the diagonal elements of the total Hamiltonian including the interaction between the continuum electron and the ion.

We have paid particular attention to an accurate evaluation of the asymptotic contributions to the Slater integrals. Outside the ion the numerical solution is fitted to the regular and irregular solutions of the Coulombic Dirac equation. The asymptotic parts of integrals can then be transformed into integrals over products of Whittaker's functions which can be analytically integrated [35].

An energy normalized solution

$$\langle\Phi_{\Gamma' E'}|\Phi_{\Gamma E}\rangle = \delta_{\Gamma'\Gamma}\delta(E' - E) \tag{A7}$$

of Eq. (A5) is given by [18]

$$|\Phi_{\Gamma E}\rangle = \sum_{\alpha=1}^{N_c}\left(|\phi_{\alpha E}\rangle + \sum_{\beta=1}^{N_c} \mathrm{P}\int \frac{|\phi_{\beta E'}\rangle\langle\phi_{\beta E'}|K|\phi_{\alpha E}\rangle}{E - E'}dE'\right) U_{\alpha\Gamma}\cos\eta_\Gamma. \tag{A8}$$

Here the K matrix is a solution of the integral equation

$$\langle\phi_{\gamma' E'}|K|\phi_{\gamma E}\rangle = \langle\phi_{\gamma' E'}|V|\phi_{\gamma E}\rangle + \sum_{\gamma''=1}^{N_c} \mathrm{P}\int \frac{\langle\phi_{\gamma' E}|V|\phi_{\gamma'' E''}\rangle\langle\phi_{\gamma'' E''}|K|\phi_{\gamma E}\rangle}{E - E''}dE''. \tag{A9}$$

The energy-dependent matrix elements $U_{\alpha\Gamma}$ and the multichannel eigenphase shifts η_Γ in Eq. (A8) are solutions of the equation

$$\sum_{\beta=1}^{N_c}\langle\phi_{\alpha E}|K|\phi_{\beta E}\rangle U_{\beta\Gamma} = -\frac{1}{\pi}\tan\eta_\Gamma U_{\alpha\Gamma}, \tag{A10}$$

which diagonalizes the on-the-energy-shell K-matrix for each E.

In our computer code the K-matrix equation (A9) is solved iteratively by starting from $K = V$. This method is computationally effective, but leads to convergence problems when the absolute values of the elements of the interaction matrix V (a dimensionless quantity in this case) are close to 1. Depending on the application the V matrix is tabulated at 40 to 70 energies. The distribution of tabulated energy points is chosen to optimize the accuracy of the integral equation (A9). Usually a mixed linear-logarithmic distribution has been found to be the most effective one. Near ionization thresholds the Rydberg states make a very important contribution to Eqs. (A8) and (A9), and also to the transition amplitudes. In photoionization calculations we usually include the three lowest Rydberg states explicitly and account for the region between the third Rydberg level and the lowest continuum state (typically 0.05 eV above the threshold) using the quantum-defect method. The eigenchannel equation (A10) is solved using subroutines from standard mathematical program libraries.

The wave functions (A8) are energy normalized eigenfunctions of the total electronic Hamiltonian but do not fulfill the incoming-wave boundary condition [18]. This condition requires that asymptotically the proper multichannel scattering wave function $|\Phi^-_{\Gamma E}\rangle$ can only have an outgoing spherical wave in the multiconfiguration single-channel state $\phi_{\Gamma E}$ defined by Eq. (A3).

It can be shown in analogy to the nonrelativistic case (Ref. [18], Sec. 4) by considerations of the asymptotic limit that the incoming-wave boundary condition requires a linear transformation of the eigenchannel states (A8) which involves the coefficients

$$Z^-_{\alpha\Gamma} = \sum_{\Lambda=1}^{N_c} U_{\alpha\Lambda} \cos\eta_\Lambda \exp(-i\eta_\Lambda) U_{\Gamma\Lambda} \exp(-i\delta_\Gamma), \quad \text{(A11)}$$

where δ_Γ is the non-Coulombic Dirac-Fock phase shift. The spherical incoming-wave normalized multiconfiguration multichannel wave functions $|\Phi^-_{\Gamma E}\rangle$ are thus given by

$$|\Phi^-_{\Gamma E}\rangle = \sum_{\alpha=1}^{N_c} \left(|\phi_{\alpha E} > + \sum_{\beta=1}^{N_c} \mathrm{P} \int \frac{|\phi_{\beta E'}\rangle\langle\phi_{\beta E'}|K|\phi_{\alpha E}\rangle}{E - E'} dE' \right) Z^-_{\alpha\Gamma}. \quad \text{(A12)}$$

It is not necessary to include the Dirac-Fock phase shift δ_Γ in states (A12) if they are used for calculation of intensities of Auger lines or partial photoionization cross sections. In the calculation of angular asymmetry and spin polarization parameters [36] one however needs multichannel states which asymptotically correspond to a specific state of the ion and to a specific wave vector of the continuum electron. These states are superpositions of the spherical wave functions (A12) and the phase shifts δ_Γ have to be included either in the Z^- matrix (A11) or in the corresponding expansion coefficients. In previous multichannel calculations of Auger rates [6–8, 15] the Z^- matrix has been set equal to the unit matrix. This approximation is justified only when the kinetic energy of the Auger electrons is large. For low kinetic-energy transitions the Z^- matrix (except for the phase shifts δ_Γ) must even be included in the calculation of line intensities or partial photoionization cross sections. In Fig. 2 we describe the basic structure of our present computer code. The subroutines which are needed for the calculation of autoionizing rates and electron scattering cross sections are still incomplete.

Our derivation of Eq. (A12) follows very closely Starace's [18] formulation of the nonrelativistic multichannel theory of photoionization. Another form of the multichannel equations was developed by Åberg and Howat in Ref. [1] for the calculation of partial Auger rates. Both approaches define, however, exactly the same multichannel wave functions, as we will explicitly show below.

The incoming-wave Lippman-Schwinger equation in Ref. [1] (Sec. 2) is given in terms of the T^- matrix by

$$|\Phi^-_{\Gamma E}\rangle = |\phi_{\Gamma E}\rangle + \lim_{\nu \to 0} \sum_{\beta=1}^{N_c} \int_0^\infty \frac{|\phi_{\beta E'}\rangle\langle\phi_{\beta E'}|Y^-|\phi_{\beta E}\rangle}{E - E' - i\nu} dE', \quad \text{(A13)}$$

where $Y^{-\dagger} = T^-$. First we take the limit $\nu \to 0$ in Eq. (A13) using the formula $\lim_{\nu\to 0}[\frac{\alpha(x)}{x - i\nu}] = \mathrm{P}[\frac{\alpha(x)}{x}] + i\pi\alpha(0)\delta(x)$ which is valid for an arbitrary differentiable function $\alpha(x)$. Second we eliminate the Y^- matrix using the transformations $Y^- = KZ^-$ and $Z^- = 1 + i\pi Y^-$.

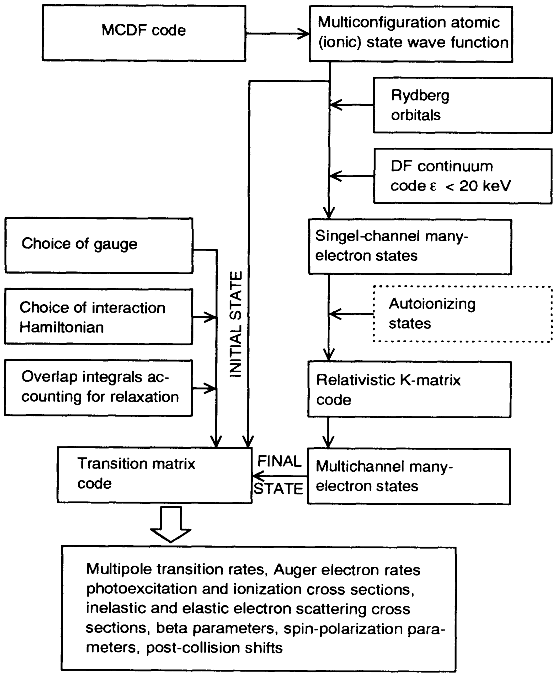

FIG. 2. A schematic diagram of the present version of the MMCDF code. The MCDF and the Rydberg state codes are modified versions of the code of Grant *et al.* [20]. The single-channel Rydberg and continuum states can be calculated in an arbitrarily defined potential, including the average-*jj* and atomic-state-function potentials used in this work. The subroutines needed for the analysis of autoionizing resonances and electron scattering are under construction.

The former transformation which is valid both on and off the energy shell is given by Eq. (2.16) in Ref. [1], and the latter on-the-energy-shell condition by one of Eqs. (2.13). Equations (2.13) also show that

$$Z^- = (1 + S^\dagger)/2. \tag{A14}$$

This procedure results in Eq. (A12) with the Z^- matrix defined in terms of the S matrix. Using the asymptotic representation of the wave function (A12) it can be shown (See Ref. [18], Sec. 4) that the scattering matrix S in Eq. (A14) is given by

$$S^\dagger_{\alpha\beta} = \sum_\Gamma U_{\alpha\Gamma} e^{-2i\eta_\Gamma} U_{\beta\Gamma}. \tag{A15}$$

Since U is an orthogonal matrix Eq. (A14) can be expressed as $Z^- = (U\tilde{U} + S^\dagger)/2$ which is identical to expression (A11) of Z^- except for the phase shifts δ_Γ. In Ref. [1] the corresponding nonrelativistic phase shifts were included in the expansion coefficients of the angle-resolved incoming-wave-normalized multichannel wave functions. This completes the proof that the multichannel of approaches of Starace [18] and of Åberg and Howat [1] are identical as they should be.

[1] T. Åberg and G. Howat, in *Encyclopedia of Physics*, edited by S. Flügge and W. Mehlhorn (Springer, Berlin, 1982), Vol. 31, p. 469.

[2] W. Mehlhorn, in *Atomic and Inner Shell Physics*, edited by B. Crasemann (Plenum, New York, 1985).

[3] M. Ya. Amusia, *Atomic Photoeffect* (Plenum, New York, 1990), Chap. 6.

[4] J. Tulkki, G. B. Armen, T. Åberg, B. Crasemann, and M. H. Chen, Z. Phys. D **5**, 241 (1987); G. B. Armen, J. Tulkki, T. Åberg, and B. Crasemann, Phys. Rev. A **36**, 5606 (1987); J. Tulkki, T. Åberg, S. B. Whitfield, and B. Crasemann, *ibid.* **41**, 181 (1990).

[5] J. Tulkki, Phys. Rev. Lett. **62**, 2817 (1989); J. Tulkki, S. Aksela, H. Aksela, E. Shigemasa, A. Yagishita, and Y. Furusawa, Phys. Rev. A **45**, 4640 (1992).

[6] G. Howat, T. Åberg, O. Goscinski, S. C. Soong, C. P. Bhalla, and M. Ahmed, Phys. Lett. **60A**, 404 (1977).

[7] G. Howat, T. Åberg, and O. Goscinski, J. Phys. B **11**, 1575 (1978).

[8] G. Howat, J. Phys. B **11**, 1589 (1978).

[9] K. R. Karim and B. Crasemann, Phys. Rev. A **31**, 709 (1985).

[10] V. Carravetta, H. Ågren, and A. Cesar, Chem. Phys. Lett. **180**, 358 (1991).

[11] S. Fritzsche , G. Zschornak, G. Musiol, and G. Soff, Phys. Rev. A **44**, 388 (1991). See also S. Fritsche, B. Fricke, and E. -D. Sepp, Phys. Rev. A **45**, 1465 (1992).

[12] S. Fritzsche and G. Zschornak, Z. Phys. D **21**, S155 (1991).

[13] S. Fritzsche and B. Fricke, Phys. Scr. **T41**, 45 (1992).

[14] D. Petrini, Can. J. Phys. **60**, 644 (1982).

[15] J. Bruneau, J. Phys. B **20**, 713 (1987).

[16] H. Kelly, Phys. Rev. A **11**, 556 (1975).

[17] J. Bruneau, J. Phys. B **16**, 4135 (1983).

[18] A. F. Starace, in *Encyclopedia of Physics*, edited by S. Flügge and W. Mehlhorn (Springer, Berlin, 1982), Vol. 31, p. 1.

[19] K. R. Karim, M. H. Chen, and B. Crasemann, Phys. Rev. A **29**, 2605 (1984).

[20] I. P. Grant, B. J. McKenzie, P. H. Norrington, D. F. Mayers, and N. C. Pyper, Comput. Phys. Commun. **21**, 207 (1980).

[21] S. Svensson, N. Mårtensson, E. Basilier, P. Å. Malmquist, U. Gelius, and K. Siegbahn, Phys. Scr. **14**, 141 (1976).

[22] A. Albiez, M. Thoma, W. Weber, and W. Mehlhorn, Z. Phys. D **16**, 97 (1990).

[23] Auger spectra of Ne and Ar have been measured at University of Oulu using electron-beam excitation and a high-resolution cylindrical mirror-type electron spectrometer (unpublished).

[24] K. G. Dyall and F. P. Larkins, J. Phys. B **15**, 2793 (1982).

[25] J. Nordgren, H. Ågren, C. Nordling, and K. Siegbahn, Phys. Scr. **19**, 5 (1979).

[26] G. C. King and F. H. Read, in *Atomic Inner-shell Physics*, edited by B. Crasemann (Plenum, New York, 1985), p. 317.

[27] D. Ridder, J. Dieringer, and N. Stolterfoht, J. Phys. B **9**, L307 (1976).

[28] T. Kondow, T. Kawai, K. Kunimori, T Onishi, and K. Tamaru, J. Phys. B **6**, L156 (1973).

[29] H. Aksela and S. Aksela, J. Phys. (Paris) Colloq. **48**, C9-565 (1987). Due to a moderate resolution of the spectrum, relative line intensities were extracted from a separate measurement (Ref. [23]).

[30] L. O. Werme, T. Bergmark, and K. Siegbahn, Phys. Scr. **8**, 149 (1973).

[31] H. Aksela, T. Mäkipaaso, V. Halonen, M. Pohjola, and S. Aksela, Phys. Rev. A **30**, 1339 (1984); H. Aksela and S. Aksela, J. Phys. (Paris) Colloq. **48**, C9-565 (1987), and references therein.

[32] A. Mäntykenttä and J. Tulkki (unpublished).

[33] E. M. Rose, *Relativistic Electron Theory* (Wiley, New York, 1961).

[34] I. P. Grant, Adv. Phys. **19**, 747 (1970).

[35] I. S. Gradshteyn and I. M. Ryzhik, *Table of Integrals, Series, and Products* (Academic, New York, 1965).

[36] K.-N. Huang, Phys. Rev. A **22**, 223 (1980).